Small Scale Wind Turbine

Jonathan Coignard[1]

[1]Technical University of Compiegne, jonathan.coignard@etu.utc.fr

Abstract — **This report aims to describe an encouraging design of small scale wind turbine. The digital modelling will allow us to have a better comprehension of the whole system. Furthermore, the digital results obtained will illustrate key points that one should mind when designing a small scale wind turbine. Finally, the experimentation on a physical system will provide reliable results.**

1. INTRODUCTION

Renewable energy sources have gained tremendous attention when seeking for independence or sustainable development. In 2011, China is the largest power generator but also the world's second largest wind power producer, almost doubling its on-grid wind capacity each year since 2005 (61 GW in 2012).

However, coal continues to be China's leading source of electricity generation, representing 66% of the installed capacity in 2012. Furthermore, a lack of transmission infrastructures decreases the absolute wind power capacity [1]. In regards to the transport sector, the electrification of the global vehicle fleet should be considered within the context of increasing urbanization as a new potential post of consumption [2].

With this frame and considering the induced environmental pollution by carbon dioxide and the depletion of conventional fuel [3], there is a growing need to produce more renewable energies. For that purpose, more efficient small scale devices and distribution services will be needed.

"Small scale wind generator" is the name given to wind generation systems with the capacity to produce less than or equal to 30kW (in Europe) or 100kW (in the United States) of electrical power [4]. Thus the top-down paradigm of electricity distribution could gradually be replaced by a bottom-up power supply [5]. We can imagine the future grid as a number of interconnected microgrids, in which every user is responsible for the generation and storage of energy consumed, and would also be able to share with neighbors [4]. The small scale wind turbines would be integrated in a smart microgrid, which will deliver electricity using digital technology to control appliances at consumer's homes. Finally, distributed generation will need distributed storage systems to cope with energy balance, and one solution could be electrical vehicles.

In this article, we will discuss the optimization of process in small scale wind turbines. However, the implementation site has a very significant impact on the production, and studies must be conducted, especially in an urban context, to determine a specific model to be installed [6]. Multiple wind turbine devices down to very low power production are available on the market (300W wind turbine GHREPOWER) [7].

In order to understand the physical process, we will discuss the digital modelling of a small scale wind turbine through the turbine, the motor, the electrical part and the command system. Then, we will explain the different steps for the experimentation performed on a motor bench and discuss the results.

2. DIGITAL MODELLING OF A SMALL SCALE WIND TURBINE

The purpose of the digital modelling is understanding how the different parts of the wind turbine works (turbine, motor, electrical circuit). In our study, modelling is a tool at our disposal for a better understanding, and will never replace results obtained within experimentation.

The wind turbine transforms kinetic energy of wind into a mechanical rotation by means of a blade. A generator will finally output an electrical power. As the wind speed is changing, a command system is needed to reach an optimal working point and maximize the production at any wind speed (Figure 1).

2.1 Turbine modelling

The relation between incoming wind and mechanical power generated is given by the following equation.

$$p_m = \frac{1}{2} c_p \rho A v_w^3 \quad (1)$$

Where:

- p_m is the mechanical power *(W)*
- ρ is the air density *(kg/m²)*
- A is the sweep area *(m²)*
- v_w is the wind speed *(m/s)*
- c_p is the power coefficient of the wind turbine

$$c_p = \frac{P_{rotor}}{P_{wind}} \quad (2)$$

The $c_p(\lambda,\beta)$ coefficient can be written as a function of the tip speed ratio λ (3) and the blade pitch angle β which will be considered null all the time.

$$\lambda = \frac{\Omega R}{v_w} \quad (3)$$

where Ω is the rotational speed of the turbine and R=1.25m the blade radius.

The c_p functions of the different wind turbine's structures (Figure 2) show their relative efficiencies. Three bladed wind turbines show the best efficiency, however

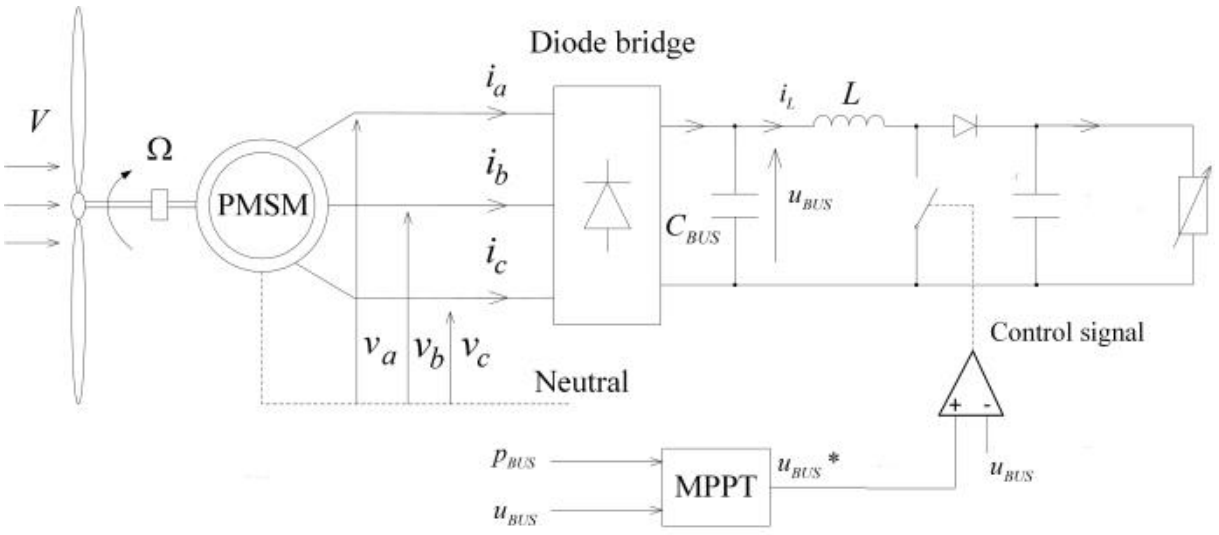

Figure 1: Proposed wind turbine design.

other wind concerns such as low speed and changing direction can lead to vertical axis models being better suited. For any structure, the Betz limit show that C_p=0.59 is a maximum value.

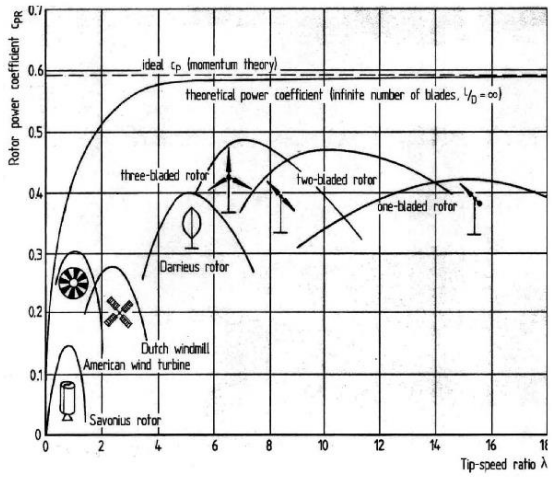

Figure 2: Power coefficient c_p for several wind turbine models.

The power coefficient can be used either from a reference table or by general equation. The wind turbine is emulated following the model of Excel 1 designed and manufactured by Bergey, where c_p can be interpolated by a 7th-order polynomial function [4]:

$$C_p(\lambda) = \sum_{k=0}^{7} a_k \lambda^k \qquad (4)$$

$a_0 = -1.9.10^{-3}$, $a_1 = 1.7.10^{-2}$, $a_2 = -1.8.10^{-2}$
$a_3 = 1.65.10^{-2}$, $a_4 = -3.1.10^{-3}$, $a_5 = 2.1.10^{-4}$
$a_6 = -4.2.10^{-6}$, $a_7 = -4.10^{-8}$.

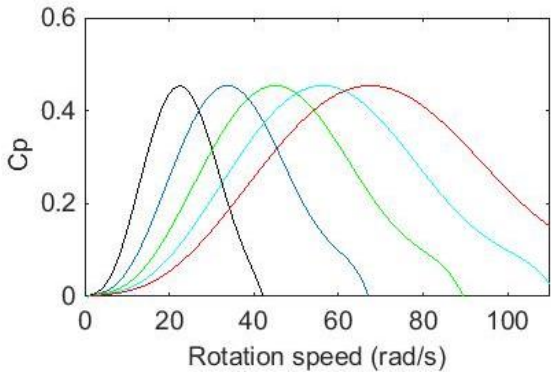

Figure 3: Representation of c_p for different wind speed (4, 6, 8, 10, 12 m/s) in function of the rotation speed (rad/s).

The power coefficient c_p describe by (4) is illustrated for five different wind speeds (Figure 3). We can see that if the wind speed increases by 2m.s^{-1} the rotation must adapt and increase by 15rad.s^{-1} to be at a maximum power coefficient. Thus, even if the potential wind power is greater with a higher wind speed, the rotation speed must be increased in order to maximize the output power. However, rapid change in the wind speed cannot be followed by the system because of its own inertia.

The inertia of the wind turbine is usually not supplied by manufacturers, and so a blade inertia can be approximated with the equations developed in [8].

$$J = k_j M L^2 \qquad (5)$$

Where L is the blade length, $M = 2.95L^{2.13}$ is the blade mass and $k_j = 0.212$. It is also important to consider an equivalent inertia if a gear box is used.

$$J_{eq} = \frac{J_{turbine}}{N^2} + J_{motor} \qquad (6)$$

where N is the gearbox coefficient. For this study we will use $J_{turbine} = 1.5\text{kg.m}^2$ and a viscos friction $F = 0.06\text{Nm/rad}$.

2.2 Motor modelling

The field of small generation was dominated by the use of asynchronous generators and more recently by Permanent Magnet Synchronous Generators (PMSG). The PMSG is popular for its efficiency as it can operate at low speed using a high numbers of poles, avoiding the need of a gearbox [4].

The stator rotation speed Ω is described by the fundamental principle of dynamic rotation:

$$c_m - c_{em} = J_{eq}\frac{d\Omega}{dt} + F\Omega \qquad (7)$$

where c_m is the aero-dynamic torque and c_{em} is the electro-magnetic torque.

The PMSG can be describe with its equivalent diagram (Figure 4), Where R_s is the phase resistance, L_s is the phase inductance and e is the electromotive force:

$$e = \sqrt{2}E.sin(\omega_e t + \varphi) \qquad (8)$$

$$E = \phi_m\, \omega_e \qquad (9)$$

$$\omega_e = p\Omega \qquad (10)$$

where ϕ_m is the flux linkage of the magnets, p is the number of poles and φ is the phase delay. Therefore the output simple tension v_a becomes:

$$v_a = R_s i_a + L_s\frac{di_a}{dt} + e_a \qquad (11)$$

Moreover, the electro-magnetic torque can be found as follows:

$$p_{em} = e_a i_a + e_b i_b + e_c i_c \qquad (12)$$

$$p_{em} = c_{em}\Omega \qquad (13)$$

$$c_{em} = \frac{1}{\Omega}(e_a i_a + e_b i_b + e_c i_c) \qquad (14)$$

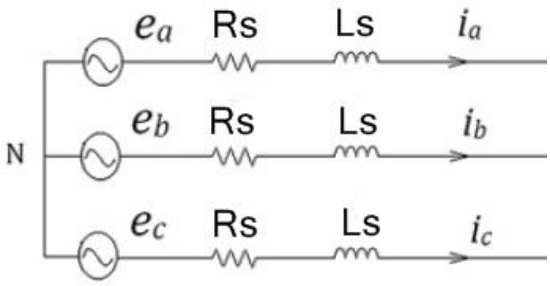

Figure 4: Electric representation of the PMSG with its corresponding parameters.

The motor itself can also be modelled using a d-q axes "Park" model [9]. However, due to the presence of an active power electronic structure (a diode bridge and a boost converter), the system become non-linear and more complex. Consequently, the SimPower system library of MATLAB/Simulink will be used to model the PMSG and the power electronic system. Nevertheless, a description of the full modelling is available [10].

SimPower system library propose several pre-set motor. It is also possible to set the parameters of a particular motor using: R_s, L_s, ϕ_m and p.

2.3 Electrical bus modelling

The PMSG output is a three-phase alternating voltage which will be converted into a constant voltage with the diode bridge. The voltage output of a diode bridge is describe in red in the Figure 5.

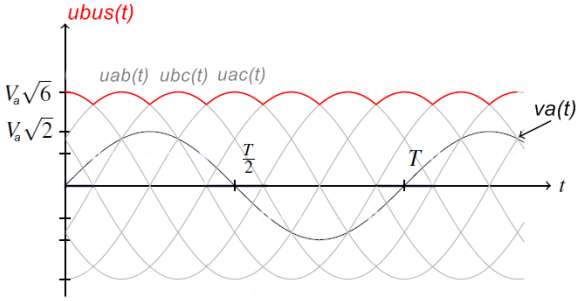

Figure 5: Output voltages of the diode bridge.

The average tension obtained can be written:

$$U_{busmoy} = \frac{3\sqrt{3}}{\pi}(\sqrt{2}V_a) \qquad (15)$$

In order to optimize the flow of energy a controllable DC-DC converter is used to obtain an active structure. The boost converter allows us to control the load imposed to the generator by controlling how much power is transmitted out of the bus. This DC-DC converter structure is used to charge a source with a greater voltage than the input voltage.

The working principal is based on the switch's states (Figure 6). When the switch is closed the current increases in the inductor (on-state), and when the switch is opened the inductor discharges in the output (off-state).

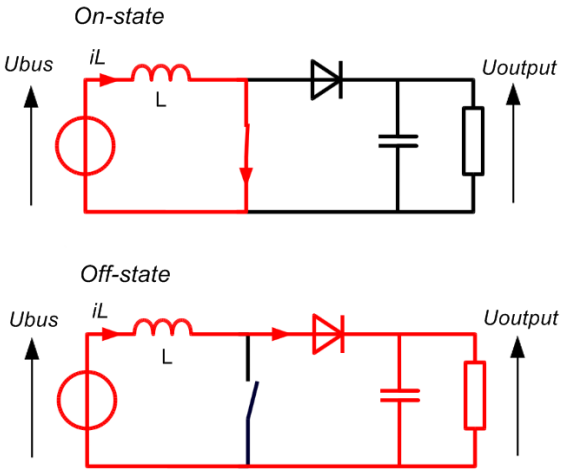

Figure 6: Working principal of the boost converter.

During the on-state i_L is described as:

$$\Delta i_L = \frac{\Delta t_{on}}{L} U_{bus} \qquad (16)$$

During the off-state i_L is described as:

$$\Delta i_L = \frac{\Delta t_{on}}{L}(U_{bus} - U_{output}) \qquad (17)$$

Figure 7 describes the voltages and currents in the different elements when switch is on and then turned off.

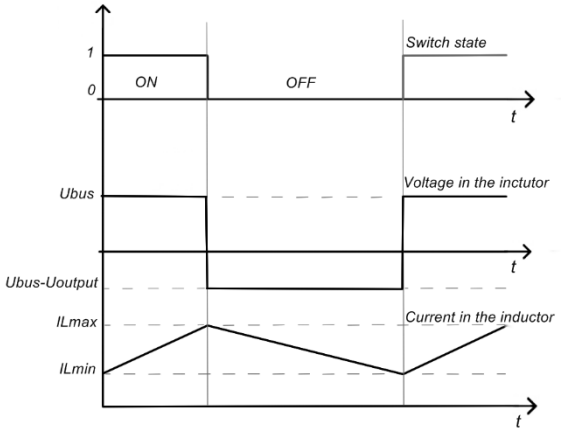

Figure 7: Inductor's current and voltage depending on the switch's state.

The controlled inductor current i_L will impose the phase currents i_a, i_b and i_c that set the electro-magnetic torque and therefore change the rotation speed. Thus, the rotation speed is controlled indirectly by the commutation of the switch.

The power electronic allows us to optimize the output power by piloting the switch on the DC bus.

2.4 Maximum power point tracking (MPPT) algorithm

In order to extract the maximum power, introducing the Maximum Power Point Tracking (MPPT) is essential. There are two types of MPPT: a direct method and an indirect method. The direct type is based on a perturbation and an observation of the system in real-time. The indirect type is based on the knowledge of the parameters of the small scale wind turbine [4]. While the latter type of MPPT needs sensors or a special estimator with an accurate knowledge of the wind turbine, the former can adapt without any specific add-on. However, difficulties lie in choosing a good

value of the perturbation step on the observation time.

The algorithm underlying the Perturb and Observe method (P&O) is described in Figure 8. It has been chosen to set the voltage as one current can correspond to two different working points.

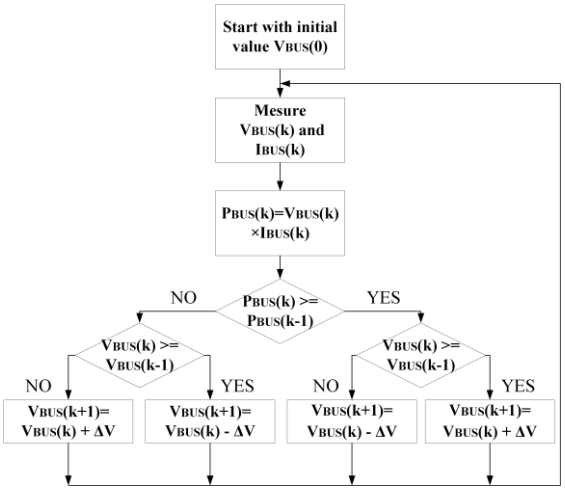

Figure 8: Flow chart of the MPPT algorithm.

In order to increase the global efficiency the perturbation step need to be variable. In the situation where the wind turbine is far from its optimum working point, the MPPT need to impulse great changes in the bus voltage. However, when the optimum working point has been reached, the MPPT must stabilize and limit oscillations (Figure 9).

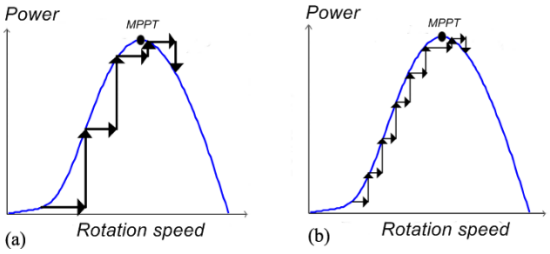

Figure 9: Number of steps needed to adjust the voltage at the MPP (a) big step and (b) small step.

There are different ways to achieve the variable step. One major drawback that can lead to the failure of the tracking process is the lack of distinction between power differences resulting from change in the wind with those resulting from the change in previous perturbation (Figure 10) [11].

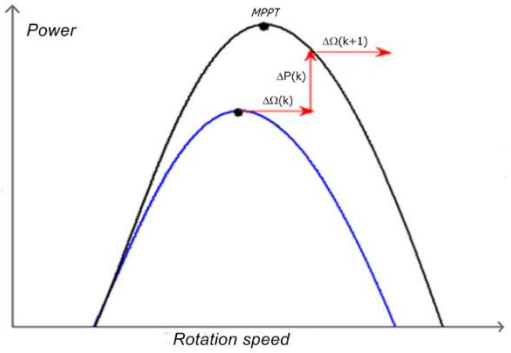

Figure 10: Misleading in the MPP research due to an increase of the power from the wind speed.

In order to adjust the variable step to any wind speed and avoid misguidance, we theoretically need to use the difference in output power regarding the difference in the power's curve slopes. Thus the reference voltage is described by the following equations:

$$\begin{cases} V_{ref}(k+1) = V_{ref}(k) + \dfrac{\Delta P_{bus}(k)}{\Delta Slope(k)} \\ Slope(k) = \dfrac{\Delta P_{bus}(k)}{\Delta V_{dc}(k)} \end{cases} \quad (18)$$

The MPPT algorithm is run every 3 seconds to ensure that the system has time to adjust the output power regarding its inertia. This observation time can be shortened depending on the time response for the maximum step that can be applied to the bus tension. It should be noticed that the MPP does not necessarily correspond with the maximum power coefficient c_{pmax} as the MPPT also takes into account the yield of the generator and the power electronics as well.

Once the reference voltage is set by the MPPT algorithm a regulator is needed to control that the system is following the

reference. Several possibilities exist; a hysteresis controller was chosen for this study instead of a PI controller because it is more robust.

A hysteresis controller is used to pilot the switch. If the reference voltage is below the actual voltage the switch will be opened, otherwise it will be closed (Figure 11).

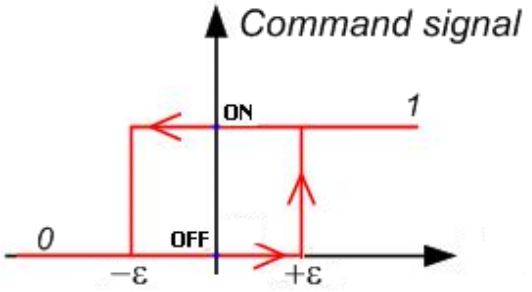

Figure 11: Working principal of the hysteresis command.

2.5 Overall diagram of the system in MATLAB/Simulink

(Figure 15)

2.6 Digital modelling results

The purpose of the results is to gain a better comprehension of the whole system, although the modelling has been validate with the physical system and shows good results (in the next chapter).

The wind turbine works without the aid of the MPPT in the beginning. Indeed we can imagine to reach a certain rotation speed before tracking the power point. This would prevent high current in the motor if the algorithm is imposing a low voltage when the wind power is important. Consequently, our simulations start at 10rad.s^{-1} (equivalent to 50V in the bus), and so the lowest wind speed to output power is 4m.s^{-1}.

It is also important to respect the dynamics of the system when running the MPPT algorithm. Due to the high inertia of the wind turbine we need at least 3s in-between each observation, to ensure system stability. Figure 12 show that with a 2s observation time oscillations are obtained. Furthermore, the maximum voltage change has been set to 5V in order to limit the peak current arising to a safe value.

In this frame, we need to optimize the MPPT algorithm to output the maximum power. Figure 13 shows a test carried for two different MPPT algorithms, blue representing the simple fix step (-5V or 5V), and red representing a variable step proportional to the power difference each step. The fix step's main drawback is to oscillate once it has reached the maximum power point, whereas the variable step is able to reach the maximum power point and maintain the same voltage in the bus (Figure 13 "bus tension" in red). However, a major problem is encounter at the 180s for the variable step (but could also have applied to the fix step). Indeed, when the wind speed (in green) is constantly increasing, the MPPT algorithm is lost. As a result the algorithm takes the wrong decision due to the lack of distinction in-between the perturbation power and the increase of the wind power.

A more sophisticated MPPT algorithm based on equation 18 has been implemented to solve misguidance when the wind power is highly variable. Figure 14 shows that the algorithm is very influenced by noise in the system, and as a result the wrong decision is made and preventing the system from reaching a maximum cp value.

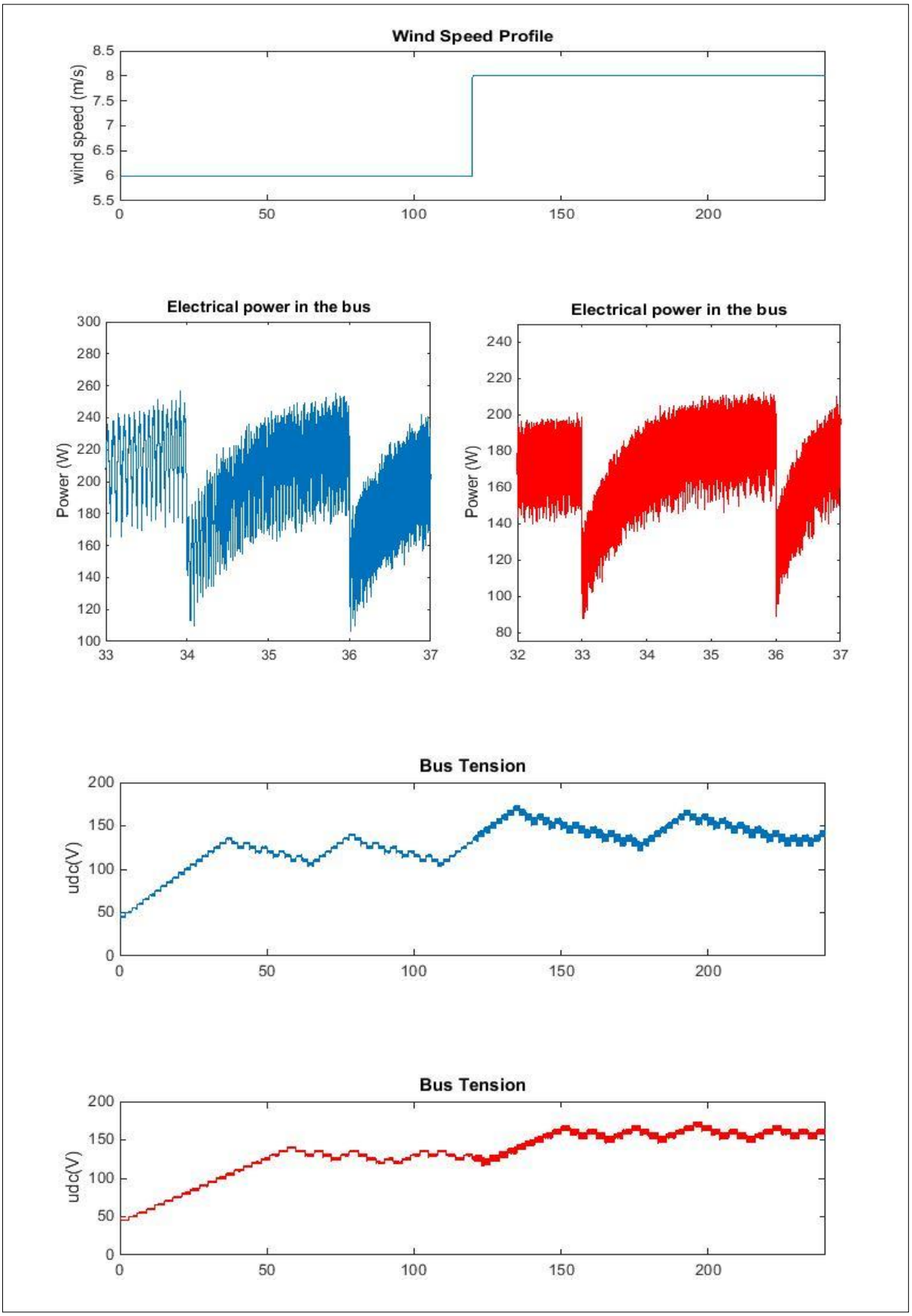

Figure 12: Experimentation with in blue a MPPT runs every 2s and in red runs every 3s (a fix step of 5V is applied).

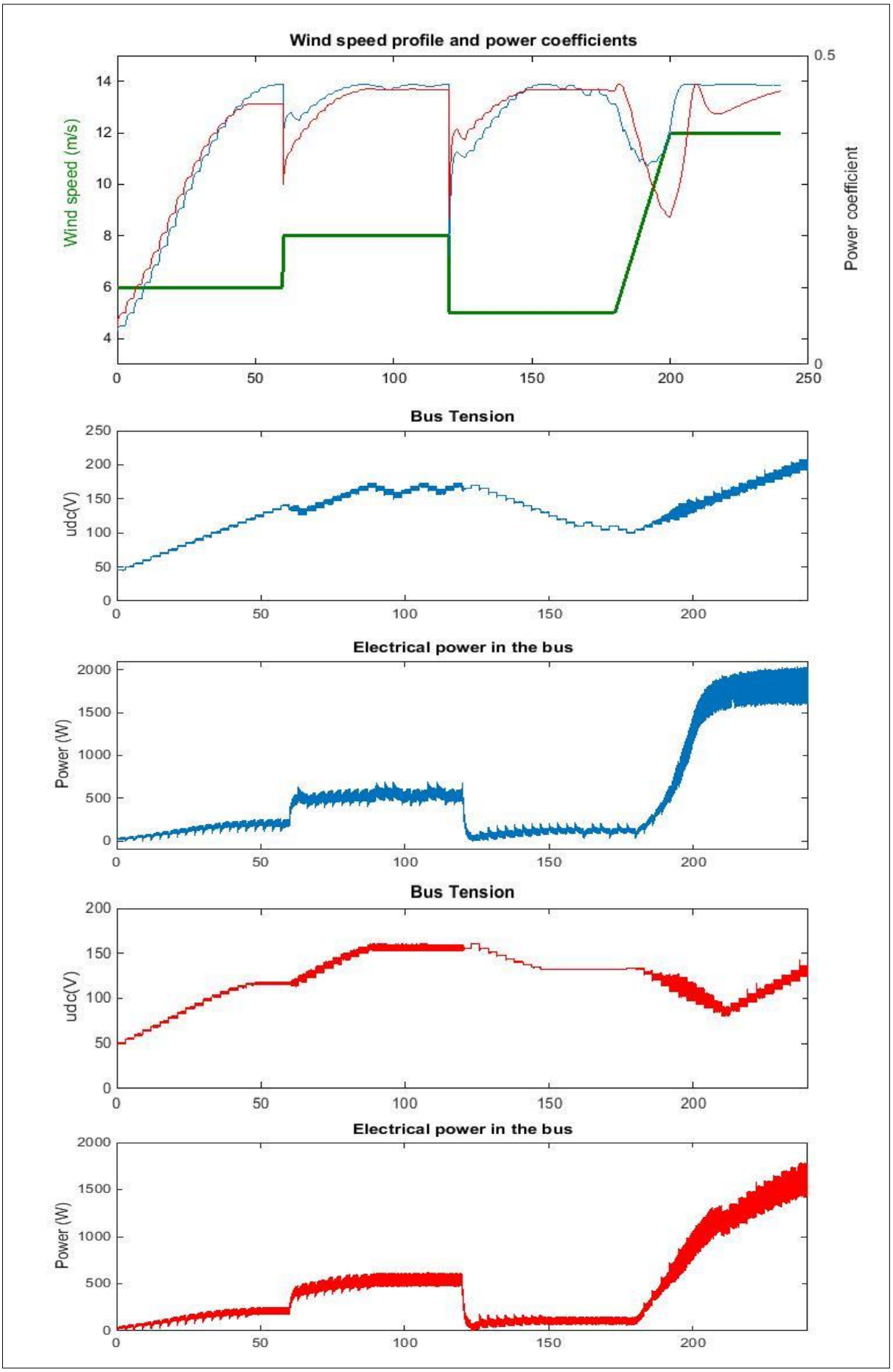

Figure 13: Experimentation of a fix step MPPT in blue and a variable step (proportional to the power difference) in red.

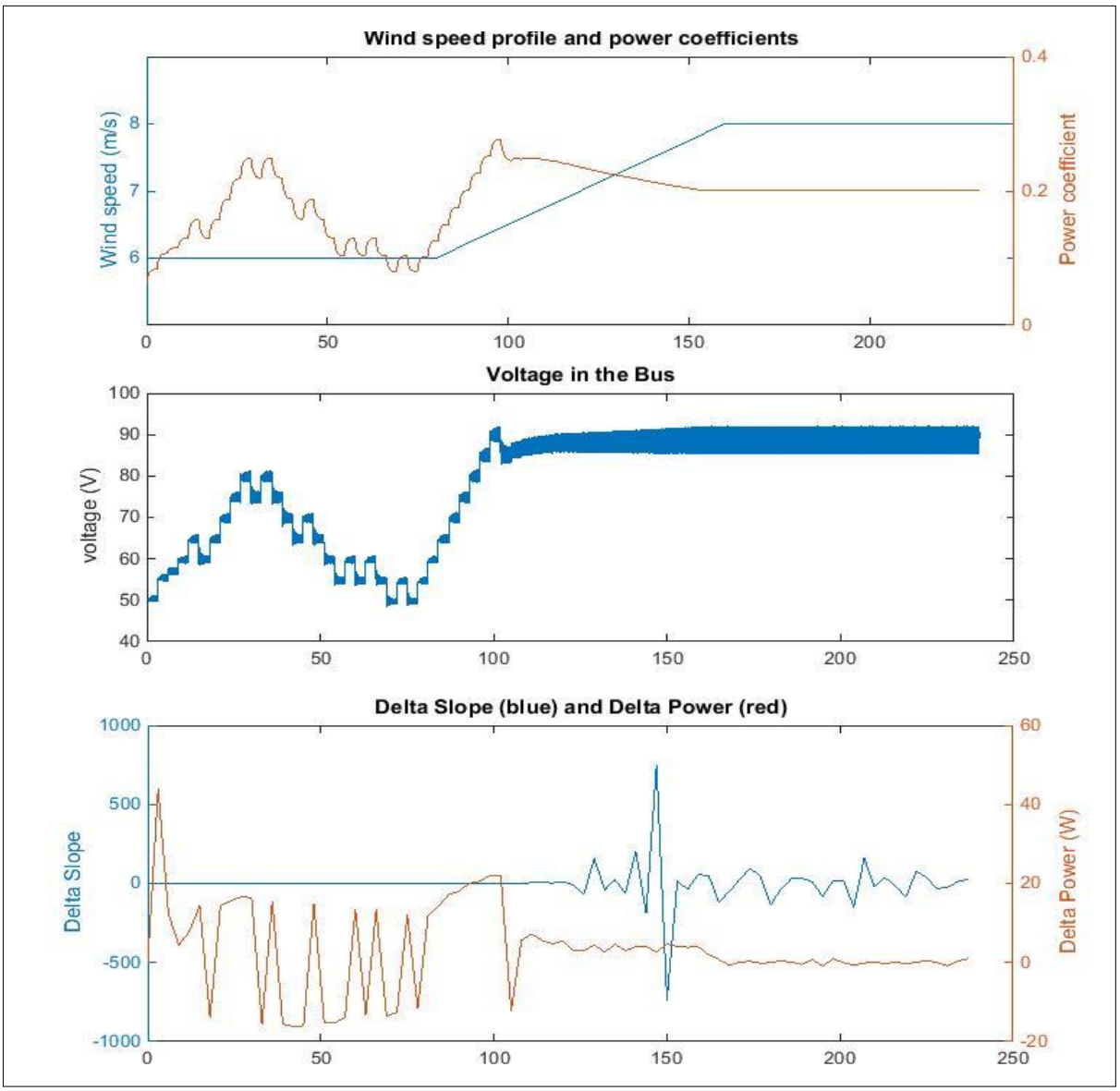

Figure 14: Digital simulation of an MPPT algorithm based on equation 18.

Figure 14 shows ΔSlope and ΔPower used in the algorithm. ΔSlope should stay close to zero as long as the wind speed is not changing. ΔPower should be close to zero only when the MPP is reached, and should have a significant absolute value, especially when the wind speed is changing. ΔSlope must compensate for the high ΔPower in transition periods when wind is changing, and so a difference is made between wind changes and perturbations induced. Figure 14 does not show such a behavior: ΔPower is oscillating around zero due to measurement noise instead of being positive.

Moreover the influence of ΔSlope is too strong when the wind starts increasing and remains when the wind stabilize at 8m.s^{-1}. A good MPPT algorithm will have to consider changes induced by wind and stay robust. Moreover, the last algorithm we proposed appears not to be very reactive as it is using a difference of a difference, and so a value measured 6s ago.

In future simulations, it will be necessary to simulate realistic wind profiles so that the system response regarding specific wind conditions could be understood.

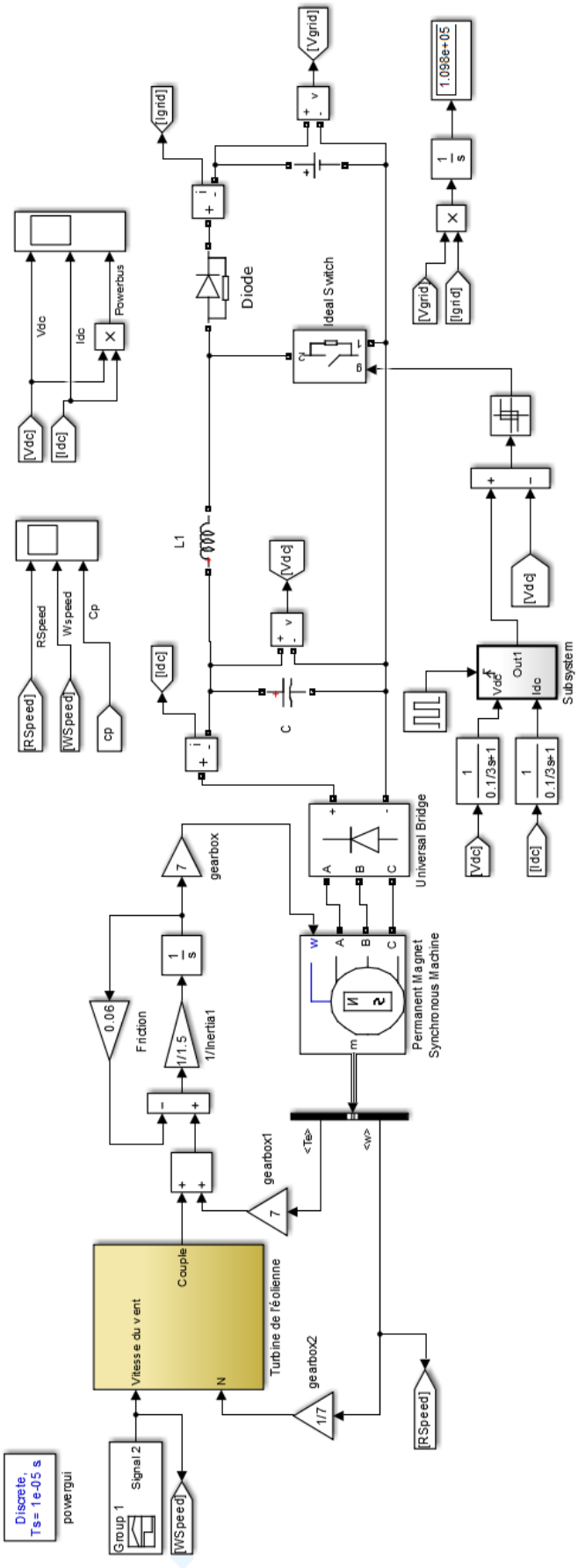

Figure 15: Simulink diagram of the digital modelling.

2 EXPERIMENTATION OF A SMALL SCALE WIND TURBINE USING A MOTOR BENCH

The purpose of the experimentation is to test the control strategy on a real system. With this experimentation we will discuss problems encountered in a more realistic setting.

In this part the system overview will be presented, with several tests of physical components in order to better understand the system. Then, obtained results will be discussed.

3.1 System overview

The schema of the system studied is given in figure 1. Wind and blades were emulated by three-phase brushless servomotor (NX430EAJR7000 from Parker) driven by a three-phase industrial inverter (C3S063V2F10 from Parker). A dSPACE DS1103 (controller board for rapid control prototyping) controlled this industrial driver in speed. The PMSM used as a generator is the same as that emulates the wind and the blades. The three-phase diode bridge was classical (SKD 51/14 from SEMIKRON). In electrical bus, capacitor CBUS=220µF and inductance L=30mH (67.5mΩ) were determined to obtain a good compromise between filtering and system dynamics. An IGBT module (SKM100GB063D from SEMIKRON) was used as a MPPT converter. It was controlled at 5 kHz by the dSPACE DS1103 via a driver (SKHI22A from SEMIKRON). The 1.1mF capacitor was the bus capacitor of DC microgrid. The power demanded by the DC microgrid was emulated by a programmable electronic load (PEL, 63202 from Chroma). PEL maintains voltage equal to 400V whatever the operating point of the small scale wind generator. Figure 16 gives a picture of the various components used.

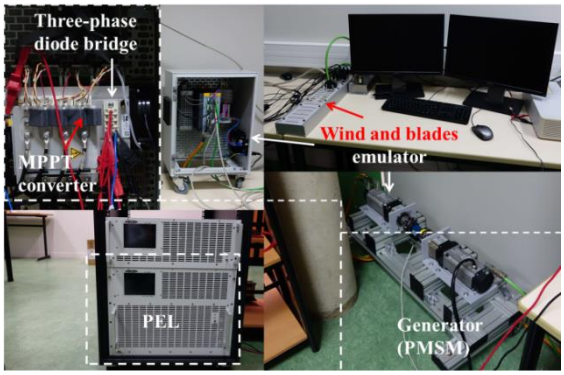

Figure 16: Photos of the physical system.

The dSPACE board allowed us to take the measurements and control the devices. The signals from the dSPACE board were processed using MATLAB/Simulink.

Three parts arose in the Simulink model: the first one aimed to get all the measurements, the second emulated the rotation speed of the system (Figure 17), and the third piloted the IGBT module (Figure 18) to control the voltage in the bus and therefore the rotation speed.

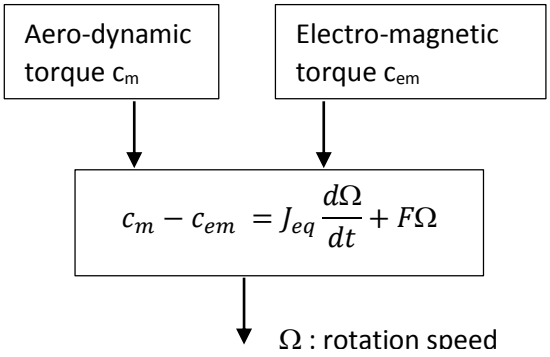

Figure 17: Schematic diagram of the Simulink model used to determine the rotation speed of the motor.

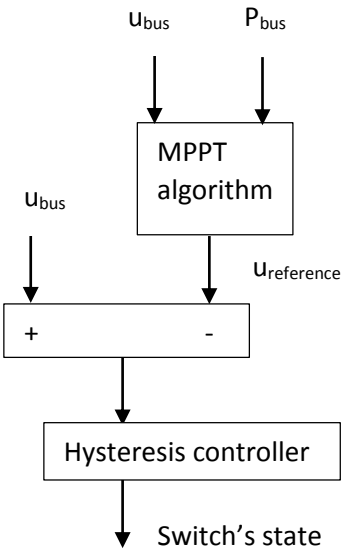

Figure 18: Schematic diagram of the Simulink model used to control the IGBT.

The Simulink model used with the real system is similar to the one used previously for the digital modelling. However, there is one difference as we cannot directly measure e_a, e_b and e_c to get the electro-magnetic power. We made the following assumption from (12):

$$p_{em} \approx v_a i_a + v_b i_b + v_c i_c$$

In order to obtain the electro-magnetic torque.

3.2 Motor's parameters and yield tests

The phase resistance was measured R_s=1.46Ohm after having warmed up the motor for an hour. The flux linkage of the magnets was measured during an off-load test, the output sinusoidal voltage has given in average ϕ_m=0.393. Finally we measured the self and the mutual inductance in average L_s=0.0051H and M_s=0.0005H.

The yield of the motor and the diode bridge was tested for different rotation speeds under different supply powers. It is shown that for a specific rotation speed the motor and the diode bridge have their own MPP (Figure 19). This is why the MPPT algorithm is not necessary at the cp_{max} but find a compromise between cp and the other yields.

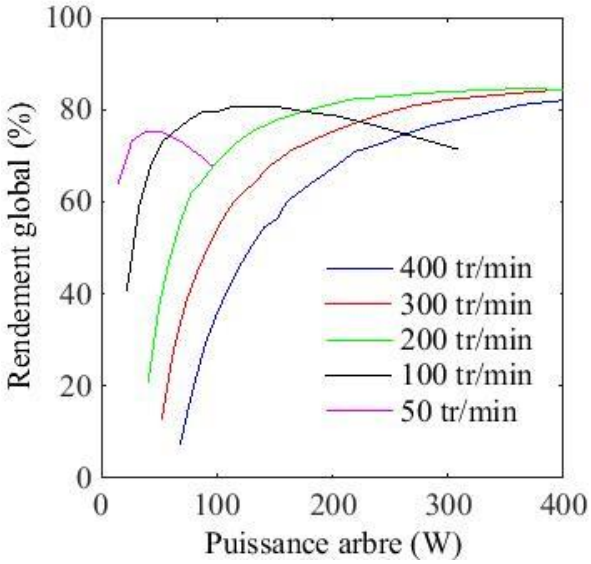

Figure 19: Yield of the motor and the diode bridge for 5 different wind speeds in function of the mechanical input power.

3.3 Experimental results

The following results aim to validate the behavior of the digital modeling according with the physical system.

The digital modeling shows good results concerning the output power, however the working point is different for the two simulations. The real system has a higher voltage output and so a higher rotation speed when the modeling has instead a greater output current. The real system acts as if its cp(λ) curve would have been shifted toward higher λ values.

It is important to note that simulation cannot reproduce exactly the same behavior as the real system just after the wind speed change. Indeed both systems are unstable and their responses depend on the previous voltage perturbation.

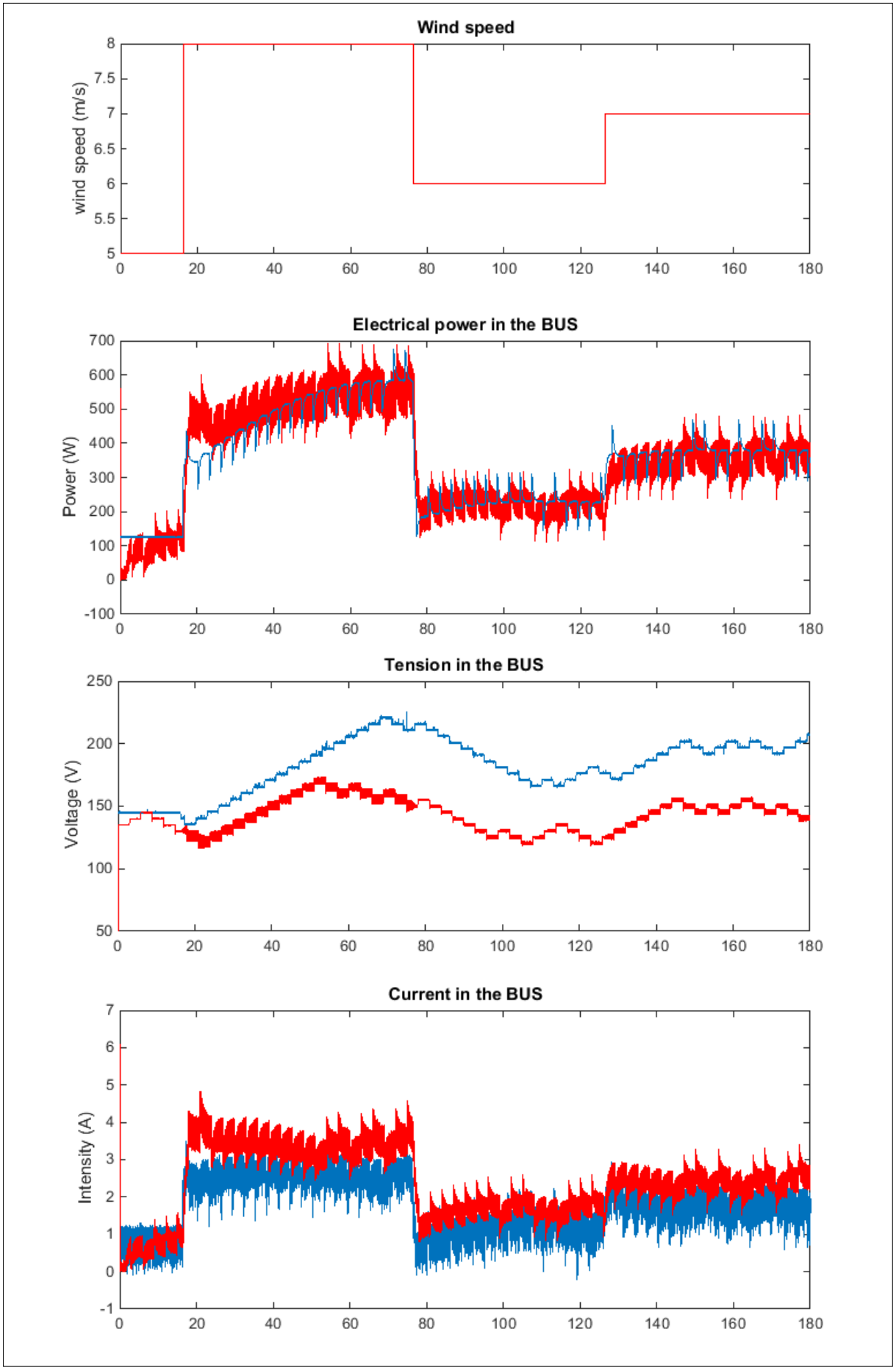

Figure 20: Comparison between experimental result (in blue) and the digital modeling (in red).

3. CONCLUSION

The systems underlying in small scale wind turbines has been explained, moreover the digital simulation allowed us to enlighten several key points:

- The MPPT should start once the turbine reached a certain rotation speed (10rad.s^{-1})
- The MPPT processing time should agree with the system mechanical dynamic (3s).
- The maximal voltage change in the bus must not overpass a safety value (5V)
- The MPPT algorithm must stabilize itself once it has reached a maximum output power
- The MPPT algorithm should not be misguide by constant variations in the input wind power nor by noise in the system

Further work needs to be carried out on variable step MPPT algorithm that can meet above exigencies. In the future, we could begin to develop system that could adapt the MPPT algorithms used depending on if the wind is steady or highly changing, based on voltage and current measurement. In any case, algorithms must be tested under realistic wind conditions on a physical system.

REFERENCES

[1] U.S Energy Information Administration EIA (http://www.eia.gov/countries/cab.cfm?fips=ch) chine

[2] Understanding the Electric Vehicle Landscape to 2020, IEA, April 2013 (www.iea.org/publications/globalevoutlook_2013.pdf)

[3] Trends in global CO2 emissions: 2013 Report, PBL Netherlands Environmental Assessment Agency, (http://www.pbl.nl/en/publications/trends-in-global-co2-emissions-2013-report)

[4] H. Al-Ghossini, H. Liu, F. Locment, M. Sechilariu, Estimation of speed rotation for MPPT used by small scale wind generator integrated in DC microgrid, 2014, laboratory Avenue-GSU.

[5] Guerrero, J. M., Chandorkar M., Lee, T-L., & Loh, P. C. (2013). Advanced Control Architectures for Intelligent MicroGrids, Part I: Decentralized and Hierarchical Control. I E E E Transactions on Industrial Electronics, 60(4), 1254-1262 .10.1109/TIE.2012.2194969

[6] Location, location, location Domestic small-scale wind field trial report, July 2009, energy saving trust (http://eprints.soton.ac.uk/353113)

[7] Small Wind World Report 2014, WWEA, 2014 (http://www.wwindea.org/wwea-releases-summary-of-2014-small-wind-world-report-update-2/)

[8] A.G. González Rodríguez, A. González Rodríguez and M. Burgos Payán, Estimating Wind Turbines Mechanical Constants.

[9] A. A. Ahmed, K. M. Abdel-Latif, M. M. Eissa, S. M. Wasfy and O.P. Malik, Study of Characteristics of Wind Turbine PMSG With Reduced Switches Count Converters

[10] A.Urtasun, P. Sanchis, I. San Martín, J. López, L. Marroyo, Modeling of small wind turbines based on PMSG with diode bridge for sensorless maximum power tracking, 2012.

[11] Abdullah M.A., Yatim A.H.M.a, Tan C.W., Saidur R., A review of maximum power point tracking algorithms for wind energy systems, 2012.